sensors

Article

Consistency and Discrepancy between Visibility and $PM_{2.5}$ Measurements: Potential Application of Visibility Observation to Air Quality Study

Ye Fei, Jie Liao * and Zhisen Zhang

National Meteorological Information Center (NMIC), China Meteorological Administration (CMA), Beijing 100081, China
* Correspondence: liaoj@cma.gov.cn; Tel.: +86-10-68408812

Abstract: High-quality measurements of air quality are the highest priority for understanding widespread air pollution. Visibility has been widely suggested to be a good alternative to $PM_{2.5}$ concentration as a measure. In this study, the similarities and differences between visibility and $PM_{2.5}$ measurements in China are checked and the results reveal the potential application of visibility observation to the study of air quality. Based on the quality-controlled $PM_{2.5}$ and visibility data from 2016 to 2018, the nonparametric Spearman correlation coefficient (ρ) values between stations for $PM_{2.5}$ and visibility-derived surface extinction coefficient (b_{ext}) decrease as the station distance (R) increases. Some relatively low ρ values (<0.4) occur in regions characterized by the lowest (background) levels of $PM_{2.5}$ and b_{ext} values, for example, the Tibetan and Yungui Plateau. The relatively lower ρ for b_{ext} compared to $PM_{2.5}$ is probably caused by the predefined maximum threshold of visibility measurements (generally 30 km). A significant correlation between $PM_{2.5}$ and b_{ext} is derived in most stations and relatively larger ρ values are evident in eastern China (Northeast China excluded) and in winter (the national median ρ is 0.67). The abrupt changes in specific mass extinction efficiency (α_{ext}) imply a potentially large influence of alternation of visibility sensors or recalibrations on visibility measurements. The b_{ext} data are thereafter corrected by comparison to the reference measurements at the adjacent stations, which leads to a three-year quality assured of visibility and b_{ext} datasets.

Keywords: $PM_{2.5}$; visibility; surface extinction coefficient; abrupt changes; dataset

check for updates

Citation: Fei, Y.; Liao, J.; Zhang, Z. Consistency and Discrepancy between Visibility and $PM_{2.5}$ Measurements: Potential Application of Visibility Observation to Air Quality Study. *Sensors* **2023**, *23*, 898. https://doi.org/10.3390/s23020898

Academic Editor: Eric P. Achterberg

Received: 21 November 2022
Revised: 28 December 2022
Accepted: 31 December 2022
Published: 12 January 2023

1. Introduction

As a byproduct of rapid and energy-intensive economic development, a huge amount of precursors and particles are emitted into the atmosphere. Anthropogenic emissions, working with natural emissions such as dust and biomass burning, lead to a thick layer of extensive haze covering thousands or tens of thousands of acres. Large areas of haze occur all over the world but are more often observed in developing countries. For example, a dense blanket of polluted air often occurs in eastern China, especially over the North China Plain in winter and in central eastern China in the crop harvest season [1–5]. Similarly, a thick brownish-gray haze often covers much of the Ganges Plain in the pre-monsoon season [6].

Measurements are the highest priority for understanding the formation and maintenance of widespread haze events and their extensive impacts. Ground measurement is the usual approach to obtaining accurate measurements of air quality indexes, among which $PM_{2.5}$ concentration (particulate matter with aerodynamic diameter < 2.5 μm) is the key component. $PM_{2.5}$ fine particles are critical because of their extensive impacts. $PM_{2.5}$ is the major factor leading to a reduction in visibility in the absence of precipitation. Visibility has reduced in the past half-century in many regions of the world owing to the increase in aerosol emissions into the atmosphere [7–9]. An increase in $PM_{2.5}$ also lead to the reduction in solar energy reaching the ground across the world from 1960 to the 1980s that was known as global dimming [10–12]. As cloud condensation nuclei, cloud formation and lifetime are intimately linked to fine particles in the atmosphere, which is the hottest debated issue in the study of climate change [13,14]. Moreover, $PM_{2.5}$ can penetrate deeply into the lungs of human beings and thereby lead to disastrous impacts on human health [15,16].

Real-time hourly $PM_{2.5}$ concentration measurements are available in many countries, which has greatly contributed to the study of air quality and related topics. The data are widely used in the following ways. (1) to study how and why air quality varies spatiotemporally [17,18]; (2) to validate model and satellite remote sensing products [19,20]; (3) to establish aerosol hygroscopic growth parameterization [21,22]; and (4) to study effects of air quality on human health [23].

Because air quality stations in mainland China are mainly located in urban areas and the spatial variability of air quality is substantial, we need extra measures to enhance the spatial coverage of national air quality networks. Local governments have established provincial air quality networks, which can, to some extent, fill the gap, but the stations are still mostly located in urban areas. Satellite imaging is widely suggested to be a potential alternative for monitoring large-scale air quality. Much effort has been paid and great progress has been made in this approach [24–26]. However, ground measurements are required by satellite remote sensing algorithms to improve their performance. Moreover, the temporal coverage of satellite retrieval is highly sensitive to the occurrence of clouds, snow, and even heavy aerosol events, all of which make image retrieval impossible [20].

Meteorological visibility is one of the operational meteorological observation parameters that reflect the abundance of solid and liquid particles in the atmosphere. The reduction in visibility is likely due to fogs or enhancements of natural and/or anthropogenic aerosols [27,28]. It is widely used as a good proxy for aerosols in the absence of rain and fog [7,29,30]. Traditionally, visibility (with units of km) is measured manually every 1–8 h, following the general rules outlined by the World Meteorological Organization. Human observation is subjective in nature, and may, therefore, eventually produce notable uncertainties. More importantly, in order to reduce cost, human observation has been gradually replaced by instrumental observation. For example, the China Meteorological Administration (CMA) established a national visibility network using a forward-scatter visibility sensor that provides hourly visibility measurements at more than 2000 automatic stations across the country [31]. This not only plays an important role in meteorological and air traffic services but is also a potential complementary network for the study of air quality. One would expect much more from this automatic observation because of the following reasons. First, automatic observation is objective in nature, which lends it good reproducibility and comparability. Second, it can provide hourly or even once-a-minute measurements. Third, automatic visibility observation can be made under harsh environments and therefore has larger spatial coverage. At the same time, these advantages are overwhelmingly dependent on good maintenance and the regular calibration of sensors.

Both measurements ($PM_{2.5}$ and visibility) are not free of measurement uncertainties and in some cases, the uncertainties may exceed the specified expectation. Many methods are thereby developed to check the data quality of meteorological and environmental data [32]. These methods mainly rely on the spatiotemporal variability of a simple variable, but one should keep in mind that it is not easy to detect true outliers from spurious data with large measurement uncertainties. Because aerosol measurements are often associated with notable uncertainties, it is strongly recommended to compare as many measurements of the same quantities as possible by different measurement techniques. This is a robust tool to assess measurement uncertainties and detect outliers. $PM_{2.5}$ measurements by the Tapered Element Oscillating Microbalance (TEOM) or the beta absorption method (BAM) represent dry particulate matter mass (RH < 40%). The visibility measured by the visibility sensor represents the ambient extinction in the atmosphere, which is related to $PM_{2.5}$ concentrations when aerosol hygroscopic growth is carefully considered. A good linear relation between $PM_{2.5}$ and the visibility-derived extinction coefficient (b_{ext}) is observed based on short-term measurements [33,34]. However, analysis of the consistency and discrepancy between $PM_{2.5}$ and visibility measurements may show a few important issues which have not been revealed by previous univariate analyses of measurement uncertainties. This tells us that caution should be taken in applying visibility measurements in the study of air quality. The rest of this paper is structured as follows. Section 2 introduces the data and method. Section 3 presents major results; and the discussion and conclusions are summarized in Section 4.

2. Data and Method

Hourly $PM_{2.5}$ and PM_{10} concentrations ($\mu g\ m^{-3}$) are available at ~1600 stations that cover at least one-year worth of measurements for the period from 2016 to 2018. The spatial distribution of the stations is shown in Figure 1, which clearly shows that the stations are clustered in urban regions, for example, 12 national stations are mainly located in urban and suburban areas of Beijing. Conversely, the visibility stations are much more evenly distributed, especially in eastern China (Figure 1). Hourly visibility data (km) are available from the National Meteorological Information Center (NMIC) of CMA at 2395 stations for the period from 2016 to 2018. Visibility is divided by 2.996 to derive the extinction coefficient (b_{ext}: Mm^{-1}) according to the instrument manual [35]. Hourly relative humidity (RH) measurements are also available from the NMIC to allow a humidity correction of b_{ext}.

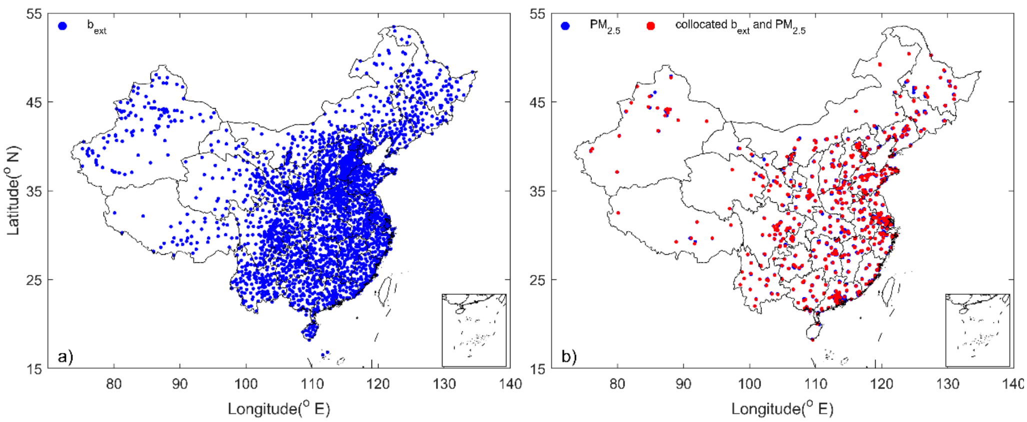

Figure 1. The spatial distribution of the visibility (b_{ext}) stations (**a**), $PM_{2.5}$ stations (blue dots in (**b**)), and collocated b_{ext} and $PM_{2.5}$ stations (red dots in (**b**)).

The data quality assurance procedure of Wu et al. [36] is adopted in this paper to provide quality control for the $PM_{2.5}$ and b_{ext} data. In general, measurements that are greatly deviated from the observations at the adjacent time or in neighboring areas or have a very low temporal variance are classified as outliers. Regular calibration of instruments and consistency between $PM_{2.5}$ and PM_{10} are checked for assurance of $PM_{2.5}$ data. For b_{ext} data, the consistency between 10 min and 1 min measurements is checked for assurance [31].

In order to check the relationship between $PM_{2.5}$ and b_{ext}, $PM_{2.5}$ measurements at stations no further than 25 km from a visibility station are averaged to match b_{ext} data. This collocation procedure trades off two requirements. One is to match $PM_{2.5}$ and b_{ext} at stations that are adjacent to each other as close as possible in order to minimize the potential effect of spatial variation; the other is to collocate substantially more b_{ext} and $PM_{2.5}$ stations for statistical analysis. Simultaneous measurements of $PM_{2.5}$ and b_{ext} are available at 502 stations (Figure 1b) that are used for the following analysis.

Spatial Spearman correlation coefficients (ρ) of $PM_{2.5}$ concentration and ambient b_{ext} between stations are calculated separately. The variation of ρ with the distance between stations (R) is studied. A few abnormally lower ρ values are found, especially for b_{ext} data in some provinces, which implies potentially larger random errors of visibility and then b_{ext} measurements than that of $PM_{2.5}$.

The linear regression between hourly $PM_{2.5}$ and b_{ext} for RH < 40% are performed to check their consistency, the slope of which represents the specific mass extinction efficiency

(α_{ext}). α_{ext} can also be calculated directly by dividing b_{ext} by $PM_{2.5}$. In some stations, α_{ext} shows a few abrupt changes that are detected by a simple but effective approach developed by Killick et al. [37]. This implies a potentially large influence of alternation of visibility sensors or re-calibrations. The visibility or b_{ext} data of the collocated 502 stations are detected and corrected by comparison to the reference $PM_{2.5}$ measurements, and thereby the visibility in these stations is set as the benchmark. The detection and correction of the remaining 1893 visibility stations should compare to the visibility measures in nearby stations. When there is a benchmark station nearby (<30 km), the visibility measurement of the benchmark station is set as the baseline. Otherwise, the regional average visibility of all meteorological stations within 100 km is set as the reference series. After all corrections are completed, a dataset consisting of three years worth of visibility and b_{ext} data is finally produced.

3. Results

Figure 2 shows the scatterplot of ρ versus R. The ρ values between two stations for $PM_{2.5}$ and b_{ext} are calculated because both quantities are not normally distributed. Not surprisingly, ρ decreases as R increases. The decay of ρ with R may be represented by an exponential equation [38].

$$\rho = \rho_0 \exp\left(-\frac{R}{R_0}\right)^{\gamma} \tag{1}$$

where the coefficient R_0 indicates the distance at which ρ decreases by a factor of e, representing the horizontal scale of the correlation. ρ_0, the zero intercept, represents ρ where the station distance is zero. The appropriate value for γ, the parameter determining how ρ decays with R, is not obvious. A range of possible values is considered that leads to substantially large variations of R_0, but not ρ_0. As suggested by Liu et al. [39], ρ_0 provides information on the uncertainty of the measurements ($\sigma^2(e)$), i.e.,

$$\sigma^2(e) = (1 - \rho_0)\sigma^2(M) \tag{2}$$

where $\sigma^2(M)$ represents the variance of the measurements. The relative uncertainty of $PM_{2.5}$ is 15% and b_{ext} is 20%, which are close to the expected measurement uncertainties. An interesting feature of Figure 2 is that some relatively lower ρ values (<0.4) are observed for R < 50 km, not only for $PM_{2.5}$ but also for b_{ext}. A further check of these low ρ values shows that they occur in regions characterized by the lowest (background) levels of $PM_{2.5}$ and b_{ext} values, for example, in the Tibetan and Yungui Plateau. This can be clearly shown by Figure 3 in which mean ρ values of $PM_{2.5}$ and b_{ext} between stations with R < 50 km are shown. Relative smaller ρ values are also found in Northeast China where $PM_{2.5}$ and b_{ext} exceed that in the Tibetan and Yungui Plateau.

ρ for visibility and, therefore, b_{ext}, between stations are smaller than that of $PM_{2.5}$, which can be evident from Figure 2 and their fitting equations. The most likely explanation is that the maximum visibility is generally set to be 30 km (about 100 M m^{-1} for b_{ext}). Given the fact that α_{ext} is about 5 m^2 g^{-1} in eastern [33] and southwest China [34], the threshold of visibility prevents visibility measurements from resolving $PM_{2.5}$ variation from a few to 20–30 μg m^{-3}. In other words, visibility data cannot reflect a subtle variation in the background level of $PM_{2.5}$ and b_{ext} as a result of their predefined maximum threshold. Therefore, it is recommended that raw b_{ext} data and visibility data be provided, which would be critical for the application of visibility data to the study of air quality study, or, more specifically, in the estimation of $PM_{2.5}$ from visibility data.

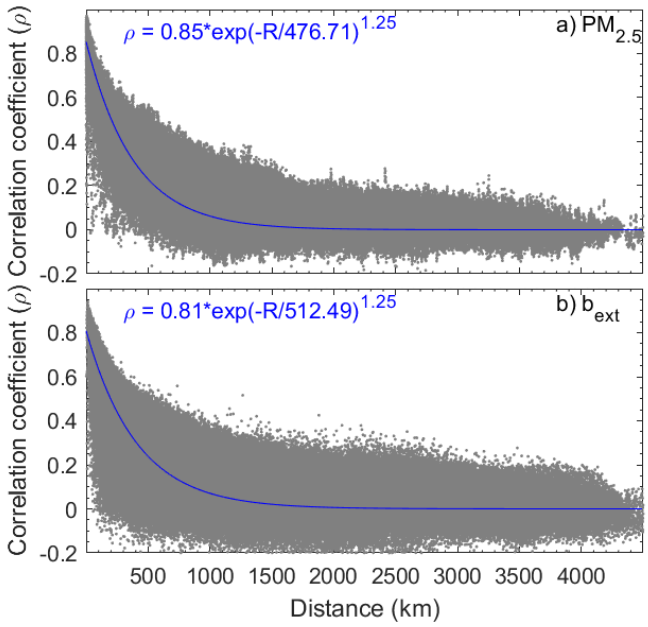

Figure 2. The scatterplot of correlation coefficient (ρ) versus station distance (R) for $PM_{2.5}$ (**a**) and b_{ext} (**b**). An exponential equation is derived to describe the relationship between ρ and R, which is also shown.

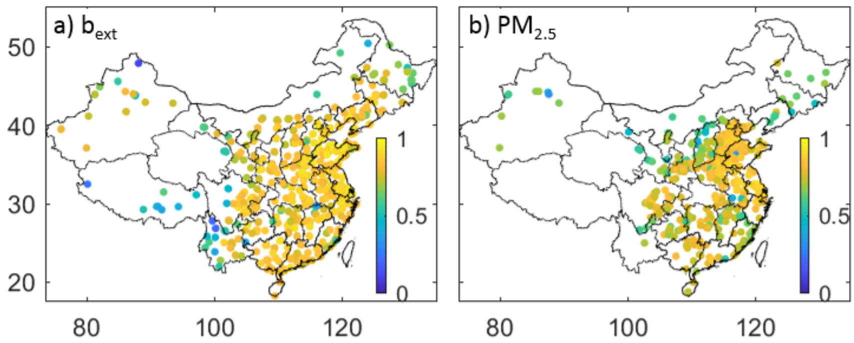

Figure 3. Spearman correlation coefficient (ρ) between stations with a distance of less than 50 km for $PM_{2.5}$ (**b**) and b_{ext} (**a**).

Figure 4 presents the seasonal spatial distribution of ρ between $PM_{2.5}$ and b_{ext} under conditions with RH < 40%, under which temporal variation of $PM_{2.5}$ should be expected to resemble that of b_{ext} because the hygroscopic growth is marginal. As summer (rainy season) match points between $PM_{2.5}$ and b_{ext} are very limited if an RH of 40% is used in eastern China, we used an RH of 60% to produce sufficient match points to perform a robust statistical analysis. In order to minimize the potential effect of hygroscopic growth, the ambient light scattering enhancement (f_{RH}) of $PM_{2.5}$ is considered by using an empirical equation below.

$$f_{RH} = 1 + \kappa \cdot \frac{RH}{(100 - RH)} \tag{3}$$

where κ is set to 0.096 according to the reference [29].

Consistent with our expectation, a significant correlation between $PM_{2.5}$ and b_{ext} is derived in most stations. The percentages with significant correlation are 91%, 89%, 88%, and 93% from spring to winter. Relatively larger ρ values are evident in eastern China (Northeast China excluded), for example, in the Beijing-Tianjin-Hebei (BTH), the Yangtze Delta Region (YDR), and Pearl Delta Region (PDR). This is partly because of a wider range of $PM_{2.5}$ and b_{ext} variation, which leads to a larger difference in ranks of the individual element and thereby ρ. In regions with low aerosol loading, for example, in the Tibetan autonomous region, Qinghai, and Yunnan Province, relatively smaller ρ values are observed. This is likely because the measurement uncertainties prevent the very subtle variation in both quantities from detection. Poor correlations are also evident at most stations in northeastern China, which seems not to be explained by the latter cause since $PM_{2.5}$ and b_{ext} in this region generally exceed those in the Tibetan Plateau. Given the fact that visibility sensors are much more accurate for smaller visibility (<10–15 km) relative to larger visibility, this should be kept in mind when the visibility data are used to estimate $PM_{2.5}$, especially in those regions dominated by $PM_{2.5}$ concentration with tens of μg m^{-3}.

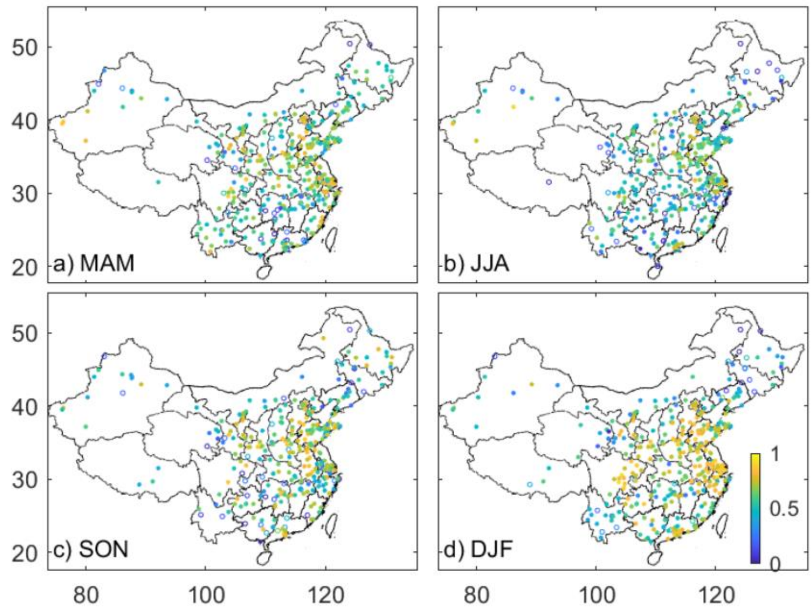

Figure 4. Spatial distribution of the Spearman correlation coefficient between $PM_{2.5}$ and visibility-derived extinction coefficient (b_{ext}). The solid (open) circle represents a significant correlation (at 99% of significance level) or not, respectively.

Seasonally, relatively larger ρ values occur in winter (the national median ρ is 0.67) and smaller ρ values are observed in summer (the national median ρ is 0.54). This is likely because the variability in $PM_{2.5}$ and b_{ext} in summer is smaller than that in winter. Furthermore, the temporal variation of aerosol chemical components, size distribution, and, therefore, the aerosol hygroscopic growth, may partly contribute to the smaller ρ values in summer, although the hygroscopic growth is considered in the analysis.

A temporal variation in the relationship between $PM_{2.5}$ and b_{ext} is evident in some stations after a closer look at the scatter plot of $PM_{2.5}$ and b_{ext} at each station. Figure 5 presents an example at Yangzhou, Jiangsu province, which shows a dramatically different relationship between $PM_{2.5}$ and b_{ext} in 2016 relative to that in 2017 and 2018. This results in a poor correlation between the two quantities. The substantial change in the $PM_{2.5}$-b_{ext} relationship may not be due to the temporal changes in aerosol compositions that mainly affects the slope of the regression analysis (i.e., α_{ext}). We can see that a dramatic change in the intercept (from ~ −47 to ~265 M m^{-1} in winter) is observed, which implies some unusual changes in the observations in one quantity but not in the other.

It is interesting to note that $PM_{2.5}$ observations at three adjacent stations (within 5 km) are close to each other and show a similar pattern in the three years of the study. Conversely, b_{ext} shows a striking phenomenon, that is, in 2016, it is extremely different from 2017 and 2018 (Figure 6). The relatively larger b_{ext} cannot be supported by contemporaneous $PM_{2.5}$ observations. $PM_{2.5}$ in these three years at these three stations shows a consistent and stable variation. The abnormally high b_{ext} in 2016 is very likely owing to the calibration or replacement of the visibility sensor, although this needs to be checked against the metadata.

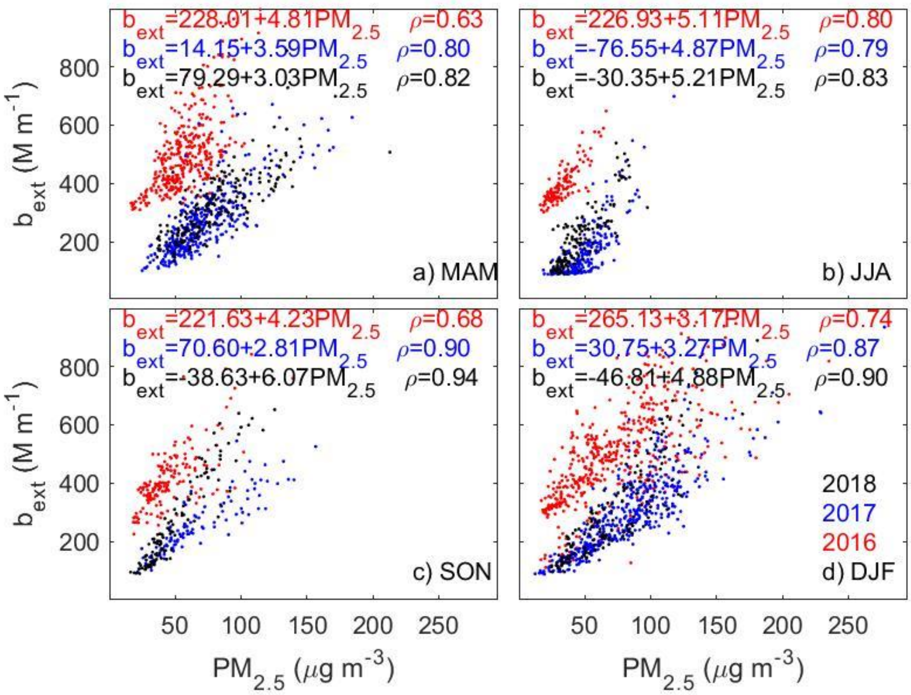

Figure 5. The scatter plot of seasonal matched points of $PM_{2.5}$ and b_{ext} in different years at Yangzhou, Jiangsu province.

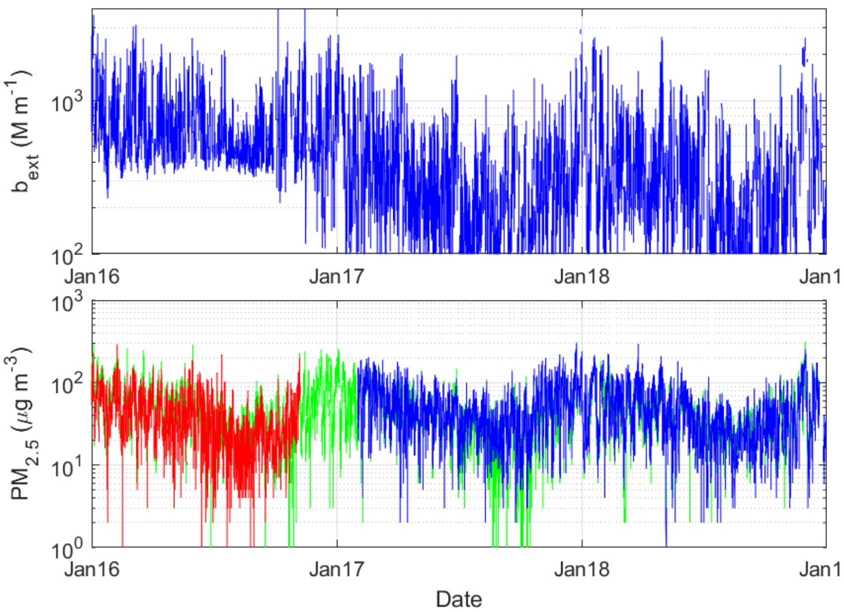

Figure 6. Time series of b_{ext} (**upper**) at Yangzhou, Jiangsu Province, and $PM_{2.5}$ (**bottom**) in three adjacent stations.

Abrupt changes in visibility and thereby b_{ext} are also evident from another perspective. Figure 7 presents the time series of the ratio of station b_{ext} to the regional mean b_{ext} in Tianjin, a municipal city near Beijing. A sudden drop in b_{ext} values occurred at stations 04, 07, 10, and 12 at the beginning of 2018, which cannot be reflected by $PM_{2.5}$ measurements (Figure 8). Since the stations are located in a very small region, this abrupt and inconsistent change of b_{ext} is very likely associated with the recalibration or alternation of the sensors.

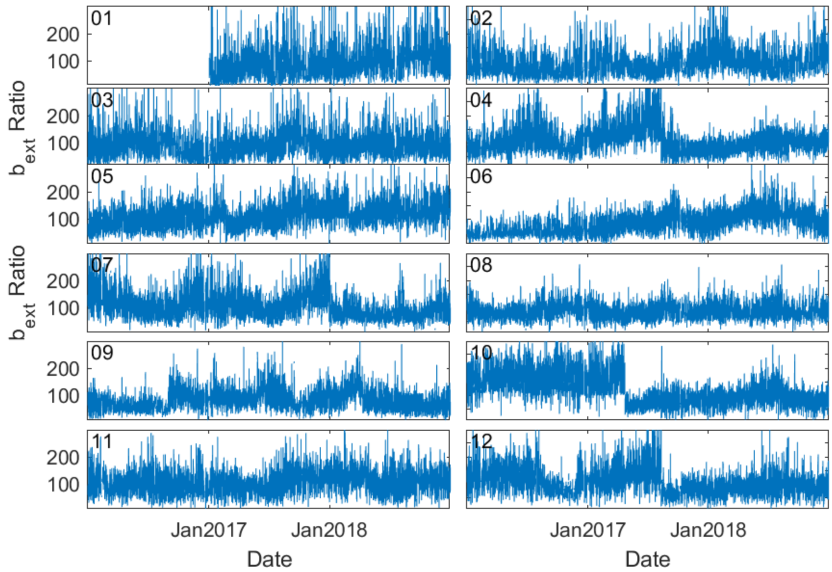

Figure 7. Time series of the ratio of b_{ext} at an individual station to the regional mean in Tianjin, a municipal city near Beijing.

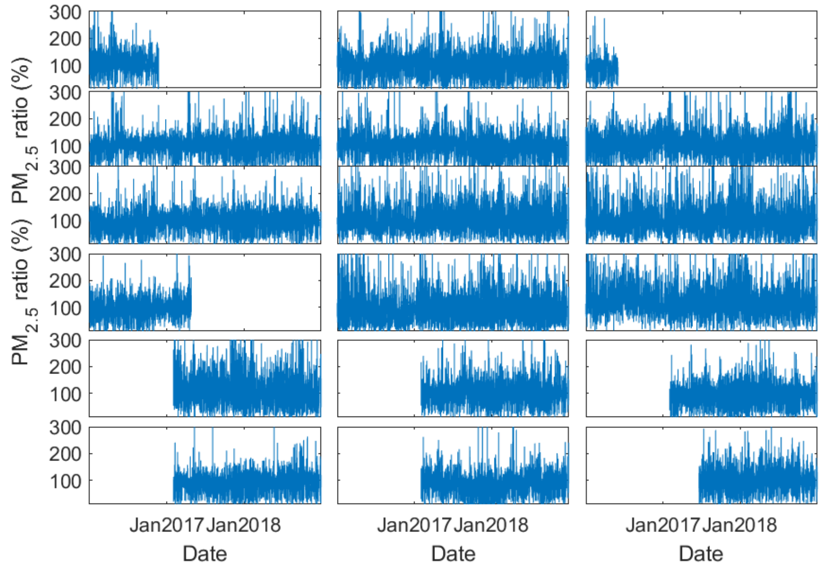

Figure 8. As Figure 7 but for $PM_{2.5}$ data at 18 stations in Tianjin.

Given the fact that $PM_{2.5}$ is stable but visibility, and hence b_{ext}, drifts with time, the time series of α_{ext} should show abrupt change points. Therefore, a simple but effective method developed by Killick et al. [37] is used to detect those change points. This method can detect abrupt changes in the mean, variance, and trend of the time series; we only detect the change points of the mean values of α_{ext} here. Figure 9 presents an example of this analysis. The value of α_{ext}, i.e., the ratio of b_{ext} to $PM_{2.5}$ under RH < 40%, shows two change points (Figure 9d), which can be also clearly shown by the scatter plot of $PM_{2.5}$ and b_{ext} (Figure 9a). Since α_{ext} values during the first two periods are abnormally higher than the expectation, indicating the abnormal measurement of b_{ext} (Figure 9b), b_{ext} measurements are then corrected by taking the measurements during the third period as the benchmark. Linear regression between b_{ext} and $PM_{2.5}$ during the three periods is performed, leading to three linear equations. The questionable b_{ext} values during the first two periods are then corrected by using the following equations.

$$b^{i}_{ext} = b^{i}_{ext} \cdot \frac{A_r + B_r \cdot PM^{i}_{2.5}}{A_i + B_i \cdot PM^{i}_{2.5}} \tag{4}$$

where i is the first or second period, and A_i and B_i represent the intercept and slope of the linear equation for the first or second period. The intercept and slope of the linear equation for the third period, the reference period, are represented by A_r and B_r, respectively. The corrected result is shown in Figure 9b, which shows a much better correlation between b_{ext} and $PM_{2.5}$ (0.87) than before (0.57) (Figure 9a). As shown in Figure 10, the time series of the ratio of corrected b_{ext} at an individual station to the regional mean in Tianjin are much more homogeneous compared to the series in Figure 7.

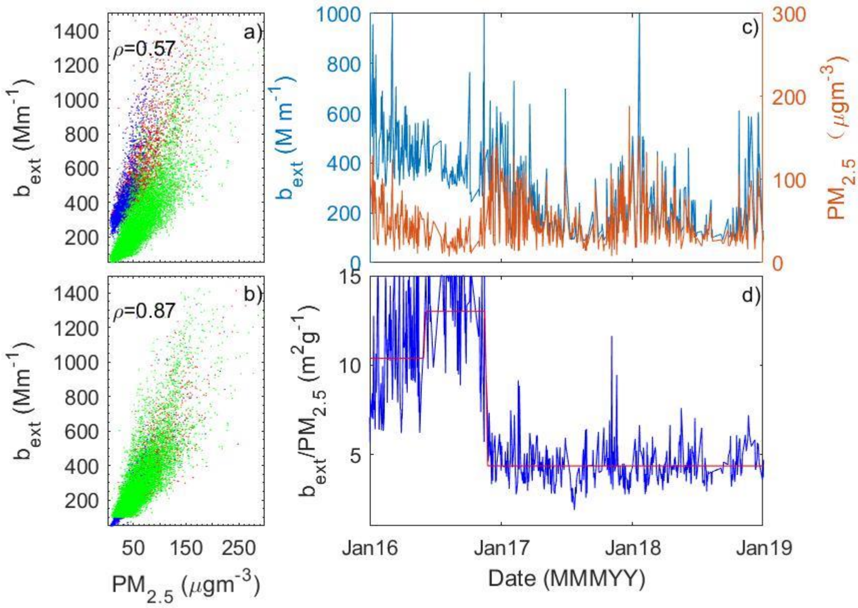

Figure 9. The relationship between $PM_{2.5}$ and b_{ext} at Yangzhou, Jiangsu Province based on original and corrected measurements (**a**,**b**); the time series of $PM_{2.5}$ and b_{ext} (**c**) and the ratio of b_{ext} to $PM_{2.5}$, i.e., α_{ext} (**d**).

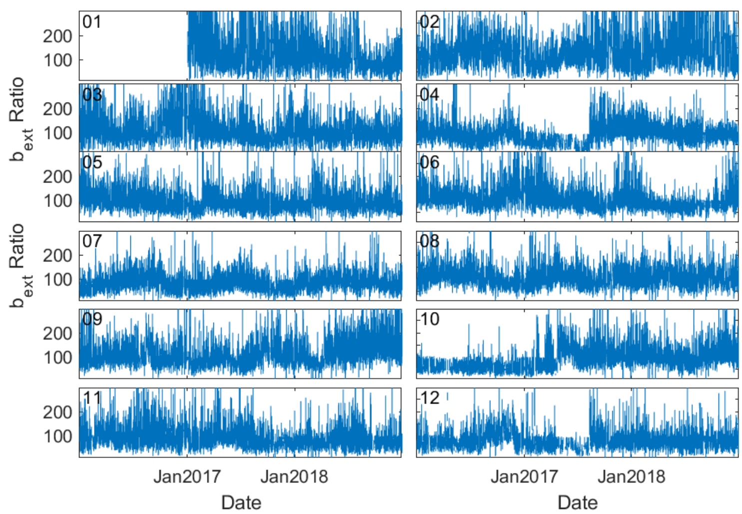

Figure 10. As Figure 7 but with b_{ext} corrected by using the method introduced in the text.

The method above is also suitable for the correction of visibility. Based on the method developed above, the visibility or b_{ext} data of the selected 502 stations are detected and corrected by comparison to the reference $PM_{2.5}$ measurements, and, therefore, the visibility in these stations is set as the benchmark. In addition to the 502 collocated stations, the corrections of the 1893 remaining visibility stations should be related to nearby visibility measurements. If there is a benchmark station nearby (<30 km), the visibility adjustment in the target station refers to the benchmark station. Otherwise, the regional average visibility of all meteorological stations within 100 km in diameter is set to the reference series. After all corrections are completed, a dataset consisting of three years worth of visibility and b_{ext} data is finally produced.

4. Discussion and Conclusions

An analysis of the similarities and differences between visibility and $PM_{2.5}$ measurements shows implications for the potential application of visibility observation to the study of air quality. Based on the quality-controlled $PM_{2.5}$ and visibility data from 2016 to 2018, the nonparametric Spearman ρ value between two stations for $PM_{2.5}$ and b_{ext} decreases as the distance between the stations, R, increases. The decay of ρ with R could be represented by an exponential equation. The relative uncertainty in $PM_{2.5}$ measurements is 15% and 20% for b_{ext}. Some relatively lower ρ values (< 0.4) observed for $R < 50$ km occur in regions characterized by the lowest (background) levels of $PM_{2.5}$ and b_{ext} values, for example, the Tibetan and Yungui Plateau. The relatively smaller ρ for b_{ext} between stations than that of $PM_{2.5}$ is probably caused by the predefined maximum threshold of visibility measurements (generally 30 km) and may be an obstacle to the application of visibility measurements in the study of air quality.

A significant correlation between $PM_{2.5}$ and b_{ext} is derived in most stations. The percentages with significant correlation are 91%, 89%, 88%, and 93% from spring to winter. Relatively larger ρ values are evident in eastern China (Northeast China excluded) and in winter (the national median ρ is 0.67). A temporal variation in the relationship between $PM_{2.5}$ and b_{ext} is evident in some stations, mainly caused by the abrupt changes in b_{ext} that are detected by an efficient approach developed by Killick et al. [37]. This implies a potentially large influence of alternation of visibility sensor instruments or re-calibrations. Therefore, the b_{ext} data are corrected by comparison to the reference measurements at the adjacent stations. A dataset of three years worth of visibility and b_{ext} data, which would be a complementary network to the study of air quality study, is finally produced.

To the best of our knowledge, this is the first time that a thorough check of the quality of automatic measurements of visibility in China has been made. Human observations of visibility in China are used by researchers to retrieve $PM_{2.5}$ concentration, which shows the great potential of visibility measurements in the study of air quality. A great development in visibility measurements in China has been the use of visibility sensors to replace human observation. Instrument-based measurements of visibility is an objective rather than subjective measure and can provide measurements with high temporal resolution. However, we should keep in mind that instrumental measurements suffer a lot of issues that require a thorough evaluation of the obtained visibility data. Data quality is of high priority for the further application of these valuable data in air quality studies. We carefully evaluate the visibility measurements by collocating them with $PM_{2.5}$ measurements in this study. It is clearly shown that visibility measurements are indeed associated with notable uncertainty. We develop a simple but effective to correct the visibility measurements. In particular, the systematic differences discussed above have been corrected at some stations. The quality of visibility data is greatly improved, which paves the way to use visibility data in air quality studies.

Author Contributions: J.L. designed the research. Y.F. and Z.Z. carried out the data processing and analysis. Y.F. wrote the first draft of the manuscript and J.L. revised the manuscript. All authors have read and agreed to the published version of the manuscript.

Funding: This research was supported by the Major Project (grant no. 42090033) and Young Scholars Project (grant no. 41905053) from the National Science Foundation of China.

Institutional Review Board Statement: Not applicable.

Informed Consent Statement: Not applicable.

Data Availability Statement: All the datasets have been made available through the national meteorological services website (http://10.1.64.154/portal/web-home.index/, accessed on 1 November 2022).

Conflicts of Interest: The authors declare no conflict of interest.

References

1. Zha, S.; Zhang, S.; Cheng, T.; Chen, J.; Huang, G.; Li, X.; Wang, Q. Agricultural Fires and Their Potential Impacts on Regional Air Quality over China. *Aerosol Air Qual. Res.* **2013**, *13*, 992–1001. [CrossRef]
2. Che, H.; Xia, X.; Zhu, J.; Li, Z.; Dubovik, O.; Holben, B.; Goloub, P.; Estelles, V.; Cuevas-Agulló, E.; Blarel, L.; et al. Column aerosol optical properties and aerosol radiative forcing during a serious haze-fog month over North China Plain in 2013 based on ground-based sunphotometer measurements. *Atmos. Chem. Phys.* **2013**, *14*, 2125–2138. [CrossRef]
3. Xia, X.; Zong, X.; Sun, L. Exceptionally active agricultural fire season in mid-eastern China in June 2012 and its impact on the atmospheric environment. *J. Geophys. Res. Atmos.* **2013**, *118*, 9889–9900. [CrossRef]
4. Sun, L.; Xia, X.; Wang, P.; Zhang, R.; Che, H.; Deng, Z.; Fei, Y.; Ran, L.; Meng, X.Y. Surface and column-integrated aerosol properties of heavy haze events in January 2013 over the North China Plain. *Aerosol Air Qual. Res.* **2015**, *15*, 1514–1524. [CrossRef]
5. Yang, Y.; Zheng, Z.; Yim, S.; Roth, M.; Ren, G.; Gao, Z.; Wang, T.; Li, Q.; Shi, C.; Ning, G.; et al. $PM_{2.5}$ Pollution Modulates Wintertime Urban-Heat-Island Intensity in the Beijing-Tianjin-Hebei Megalopolis, China. *Geophys. Res. Lett.* **2020**, *47*, e2019GL084288. [CrossRef]
6. Gustafsson, O.; Krusa, M.; Zencak, Z.; Sheesley, R.J.; Granat, L.; Engstrom, E.; Praveen, P.S.; Rao, P.S.; Leck, C.; Rodhe, H. Brown clouds over South Asia: Biomass or fossil fuel combustion? *Science* **2009**, *323*, 495–498. [CrossRef]
7. Che, H.; Zhang, X.; Li, Y.; Zhou, Z.; Qu, J.J. Horizontal visibility trends in China 1981–2005. *Geophys. Res. Lett.* **2007**, *34*. [CrossRef]
8. Zhao, P.; Zhang, X.; Xu, X.; Zhao, X. Long-term visibility trends and characteristics in the region of Beijing, Tianjin, and Hebei, China. *Atmos. Res.* **2011**, *101*, 711–718. [CrossRef]
9. Li, J.; Li, C.; Zhao, C.; Su, T. Changes in surface aerosol extinction trends over China during 1980-2013 inferred from quality-controlled visibility data. *Geophys. Res. Lett.* **2016**, *43*, 8713–8719. [CrossRef]
10. Streets, D.; Wu, Y.; Chin, M. Two-decadal aerosol trends as a likely explanation of the global dimming/brightening transition. *Geophys. Res. Lett.* **2006**, *33*. [CrossRef]
11. Xia, X.; Chen, H.; Li, Z.; Wang, P.; Wang, J. Significant reduction of surface solar irradiance induced by aerosols in a suburban region in northeastern China. *J. Geophys. Res.* **2007**, *112*. [CrossRef]
12. Wild, M. Global dimming and brightening: A review. *J. Geophys. Res.* **2009**, *114*, D00D16. [CrossRef]
13. Rosenfeld, D.; Sherwood, S.C.; Wood, R.; Donner, L.J. Climate Effects of Aerosol-Cloud Interactions. *Science* **2014**, *343*, 379–380. [CrossRef] [PubMed]
14. Fan, J.; Wang, Y.; Rosenfeld, D.; Liu, X. Review of Aerosol–Cloud Interactions: Mechanisms, Significance, and Challenges. *J. Atmos. Sci.* **2016**, *73*, 4221–4252. [CrossRef]
15. Zheng, S.; Pozzer, A.; Cao, C.; Lelieveld, J. Long-term (2001–2012) concentrations of fine particulate matter ($PM_{2.5}$) and the impact on human health in Beijing, China. *Atmos. Chem. Phys.* **2015**, *15*, 5715–5725. [CrossRef]
16. Shiraiwa, M.; Ueda, K.; Pozzer, A.; Lammel, G.; Kampf, C.J.; Fushimi, A.; Enami, S.; Arangio, A.M.; Frohlichnowoisky, J.; Fujitani, Y. Aerosol Health Effects from Molecular to Global Scales. *Environ. Sci. Technol.* **2017**, *51*, 13545–13567. [CrossRef] [PubMed]
17. Wang, Y.; Ying, Q.; Hu, J.; Zhang, H. Spatial and temporal variations of six criteria air pollutants in 31 provincial capital cities in China during 2013–2014. *Environ. Int.* **2014**, *73*, 413–422. [CrossRef]
18. Hu, J.; Wang, Y.; Ying, Q.; Zhang, H. Spatial and temporal variability of $PM_{2.5}$ and PM_{10} over the North China Plain and the Yangtze River Delta, China. *Atmos. Environ.* **2014**, *95*, 598–609. [CrossRef]
19. Han, Y.; Wu, Y.; Wang, T.; Zhuang, B.; Li, S.; Zhao, K. Impacts of elevated-aerosol-layer and aerosol type on the correlation of AOD and particulate matter with ground-based and satellite measurements in Nanjing, southeast China. *Sci. Total Environ.* **2015**, *532*, 195–207. [CrossRef]
20. Song, Z.; Fu, D.; Zhang, X.; Han, X.; Song, J.; Zhang, J.; Wang, J.; Xia, X. MODIS AOD sampling rate and its effect on $PM_{2.5}$ estimation in North China. *Atmos. Environ.* **2019**, *209*, 14–22. [CrossRef]
21. Chen, J.; Li, Z.; Lv, M.; Wang, Y.; Wang, W.; Zhang, Y.; Wang, H.; Yan, X.; Sun, Y.; Cribb, M. Aerosol hygroscopic growth, contributing factors, and impact on haze events in a severely polluted region in northern China. *Atmos. Chem. Phys.* **2019**, *19*, 1327–1342. [CrossRef]
22. Zhao, C.; Yu, Y.; Kuang, Y.; Tao, J.; Zhao, G. Recent Progress of Aerosol Light-scattering Enhancement Factor Studies in China. *Adv. Atmos. Sci.* **2019**, *36*, 1015–1026. [CrossRef]

23. Brook, R.D.; Rajagopalan, S.; Pope, C.A.; Brook, J.R.; Bhatnagar, A.; Diezroux, A.V.; Holguin, F.; Hong, Y.; Luepker, R.V.; Mittleman, M.A. Particulate Matter Air Pollution and Cardiovascular Disease An Update to the Scientific Statement From the American Heart Association. *Circulation* **2010**, *121*, 2331–2378. [CrossRef] [PubMed]
24. Engel-Cox, J.A.; Holloman, C.H.; Coutant, B.W.; Hoff, R.M. Qualitative and quantitative evaluation of MODIS satellite sensor data for regional and urban scale air quality. *Atmos. Environ.* **2004**, *38*, 2495–2509. [CrossRef]
25. Li, J.; Carlson, B.E.; Lacis, A.A. How well do satellite AOD observations represent the spatial and temporal variability of $PM_{2.5}$ concentration for the United States. *Atmos. Environ.* **2015**, *102*, 260–273. [CrossRef]
26. Fu, D.; Song, Z.; Zhang, X.; Xia, X.; Wang, J.; Che, H.; Wu, H.; Tang, X.; Zhang, J.; Duan, M. Mitigating MODIS AOD non-random sampling error on surface $PM_{2.5}$ estimates by a combined use of Bayesian Maximum Entropy method and linear mixed-effects model. *Atmos. Pollut. Res.* **2020**, *11*, 482–490. [CrossRef]
27. Yu, X.; Ma, J.; An, J.; Yuan, L.; Zhu, B.; Liu, D.; Wang, J.; Yang, Y.; Cui, H. Impacts of meteorological condition and aerosol chemical compositions on visibility impairment in Nanjing, China. *J. Clean. Prod.* **2016**, *131*, 112–120. [CrossRef]
28. Yang, Y.; Ge, B.; Chen, X.; Yang, W.; Wang, Z.; Chen, H.; Xu, D.; Wang, J.; Tan, Q.; Wang, Z. Impact of water vapor content on visibility: Fog-haze conversion and its implications to pollution control. *Atmos. Res.* **2021**, *256*, 105565. [CrossRef]
29. Wang, K.; Dickinson, R.E.; Liang, S. Clear sky visibility has decreased over land globally from 1973 to 2007. *Science* **2009**, *323*, 1468–1470. [CrossRef]
30. Gui, K.; Che, H.; Zeng, Z.; Wang, Y.; Zhai, S.; Wang, Z.; Luo, M.; Zhang, L.; Liao, T.; Zhao, H.; et al. Construction of a virtual $PM_{2.5}$ observation network in China based on high-density surface meteorological observations using the Extreme Gradient Boosting model. *Environ. Int.* **2020**, *141*, 105801. [CrossRef]
31. Fei, Y.; Fu, D.; Song, Z.; Han, S.; Han, X.; Xia, X. Spatiotemporal variability of surface extinction coefficient based on two-year hourly visibility data in mainland China. *Atmos. Pollut. Res.* **2019**, *10*, 1944–1952. [CrossRef]
32. Thorne, P.W. Revisiting radiosonde upper air temperatures from 1958 to 2002. *J. Geophys. Res.* **2005**, *110*. [CrossRef]
33. Jing, J.; Wu, Y.; Tao, J.; Che, H.; Xia, X.; Zhang, X.; Yan, P.; Zhao, D.; Zhang, L. Observation and analysis of near-surface atmospheric aerosol optical properties in urban Beijing. *Particuology* **2015**, *18*, 144–154. [CrossRef]
34. Ji, D.; Deng, Z.; Sun, X.; Ran, L.; Xia, X.; Fu, D.; Song, Z.; Wang, P.; Wu, Y.; Tian, P.; et al. Estimation of $PM_{2.5}$ Mass Concentration from Visibility. *Adv. Atmos. Sci.* **2020**, *37*, 671–678. [CrossRef]
35. Zhang, A. *Modern Meteorological Observation*, 2nd ed.; Peking University Press: Beijing, China, 2015.
36. Wu, H.; Tang, X.; Wang, Z.; Wu, L.; Lu, M.; Wei, L.; Zhu, J. Probabilistic Automatic Outlier Detection for Surface Air Quality Measurements from the China National Environmental Monitoring Network. *Adv. Atmos. Sci.* **2018**, *35*, 1522–1532. [CrossRef]
37. Killick, R.; Fearnhead, P.; Eckley, I.A. Optimal Detection of Changepoints With a Linear Computational Cost. *J. Am. Stat. Assoc.* **2012**, *107*, 1590–1598. [CrossRef]
38. Sioris, C.E.; Abboud, I.; Fioletov, V.E.; McLinden, C.A. AEROCAN, the Canadian sub-network of AERONET: Aerosol monitoring and air quality applications. *Atmos. Environ.* **2017**, *167*, 444–457. [CrossRef]
39. Liu, G.; Tarasick, D.W.; Fioletov, V.E.; Sioris, C.E.; Rochon, Y.J. Ozone correlation lengths and measurement uncertainties from analysis of historical ozonesonde data in North America and Europe. *J. Geophys. Res.* **2009**, *114*. [CrossRef]